17th World Conference on Earthquake Engineering, 17WCEE
Sendai, Japan - September 13th to 18th 2020

IMAGE ANALYSIS FOR ROAD STRUCTURE DAMAGE DUE TO THE 2018 HOKKAIDO IBURI TOBU EARTHQUAKE

K. Yoshinari [1], G. Shoji [2]

[1] *Graduate Student, Department of Engineering Mechanics and Energy, University of Tsukuba, s1920954@s.tsukuba.ac.jp*
[2] *Professor, Faculty of Engineering, Information and Systems, University of Tsukuba, gshoji@kz.tsukuba.ac.jp*

Abstract

A database was set up for 42 affected roads among 87 damaged areas in Hokkaido, Japan, including Atsuma Town, Abira Town, Mukawa Town and Tomakomai City, which were subjected to strong ground motions of the 2018 Hokkaido Iburi-Tobu earthquake [1]. On the basis of our compiled data, we chose to focus on damage to road structures caused by slope failures and road failures and performed image analysis of seven aerial photographs that encompassed those structures.

In particular, for 31 among the 87 damaged areas, the features in the images obtained by geometric correction and conversion to grey scale were classified into three categories: (A) darkened luminance uniformly distributed around affected parts of a targeted road, (B) darkened luminance within affected parts of a targeted road with brightened luminance surrounding the affected areas and (C) brightened luminance uniformly distributed around the affected areas of a targeted road. We computed threshold values for four characteristics: contrast (*CNT*), variance (*VAR*), skewness (*SKW*) and entropy (*EPY*). Finally, by using the characteristic values, we estimated the extents of the 31 damaged areas of targeted roads.

For each of the seven damaged-road monochrome aerial photographs, we set the total number of pixels in the window to $N = 729$. Then we defined the variables *CNT*, *VAR*, *SKW* and *EPY* by using the approximate value $P(l) = H(l)/N$ of the probability density of the normalised luminance value (so that the total number of pixels is 1) and obtained their histograms.

Then, assuming threshold values for each aerial photographs, we found the error between the characteristic value and the assumed threshold value in the damaged pixel and adopted the value when the sum of squares of the error was at the minimum for the threshold value. Next, we calculated the mean and standard deviation of the threshold values for each characteristic value in the aerial photograph: 7357 ± 910 for *CNT*, 422 ± 115 for *VAR*, 0.475 ± 0.182 for *SKW* and 0.633 ± 0.0239 for *EPY*.

Pixels whose absolute difference from the mean was smaller than the standard deviation were extracted as pixels representing damaged areas. *EPY*, which in theory is highly explanatory, was accurate in extracting damage in all images. In contrast, the accuracy of *CNT* was high only in aerial photographs 1 and 4, and that of *VAR* was high only in aerial photographs 2 and 4. We also found that in aerial photograph 5, *VAR* and *EPY* incorrectly detected the road as damaged because it appears dark owing to shadowing by the adjacent forest. This is an example of the issue of processing of pixels that have the same luminance distribution as damaged areas owing to reasons other than slope failure.

Keywords: damage detection, road structure, slope failure, 2018 Hokkaido Iburi-Tobu earthquake

1. Introduction

In both the 2016 Kumamoto and the 2018 Hokkaido Iburi-Tobu earthquakes, various road structures were severely damaged by ground motions and the induced slope failures. In terms of slope failures due to the 2008 Iwate-Miyagi Nairiku earthquake, Midorikawa and Miura [1] performed texture analysis using high-resolution SAR images for detecting damaged areas. Shoji and Sakurai [2] constructed a damage function for predicting the damage rate of road structures due to the slope failures of the 2008 Iwate-Miyagi Nairiku earthquake from the intensity of ground motion. Yoshinari and Shoji [3] performed texture analysis on road structures damaged by the 2018 Hokkaido Iburi-Tobu earthquake and clarified explainable characteristic values for road damage detection by slope failures.

In this study, road damage associated with the 2018 Hokkaido Iburi-Tobu earthquake is identified by analysis of seven aerial photographs and derivative imagery.

2. Data construction and damage classification

We constructed a disaster database of road structures affected by the Hokkaido Iburi-Tobu earthquake. For affected areas, we accessed cartographic line data available as basic map information from the Geospatial Information Authority of Japan [4]. We used a 10 * 10 - km mesh for the exposed-roads data. Road damage was identified directly by the analyst using the Google Disaster Information Map [5], and the data were stored as damage area centre points.

By a process to derive pixel data representing road areas, the aerial photographs are converted into mesh data (Fig. 1). The photographs first are geometrically corrected to match four or more ground control points, which are exactly known positions, such as a specific road edge or an intersection in the line data (Fig. 1a). The corrected photographs are converted to polygon data (Fig. 1b), which are then divided into meshes. The mesh size defines the pixel size for the image (Fig. 1c). The road data are captured from the polygon data (Fig. 1d) and converted to mesh data (Figs. 1e,f). By this process, we visually selected seven aerial photographs (Fig. 2, Fig. 3) to demonstrate the damage areas (17 slope failures and 3 road failures) as polygon data.

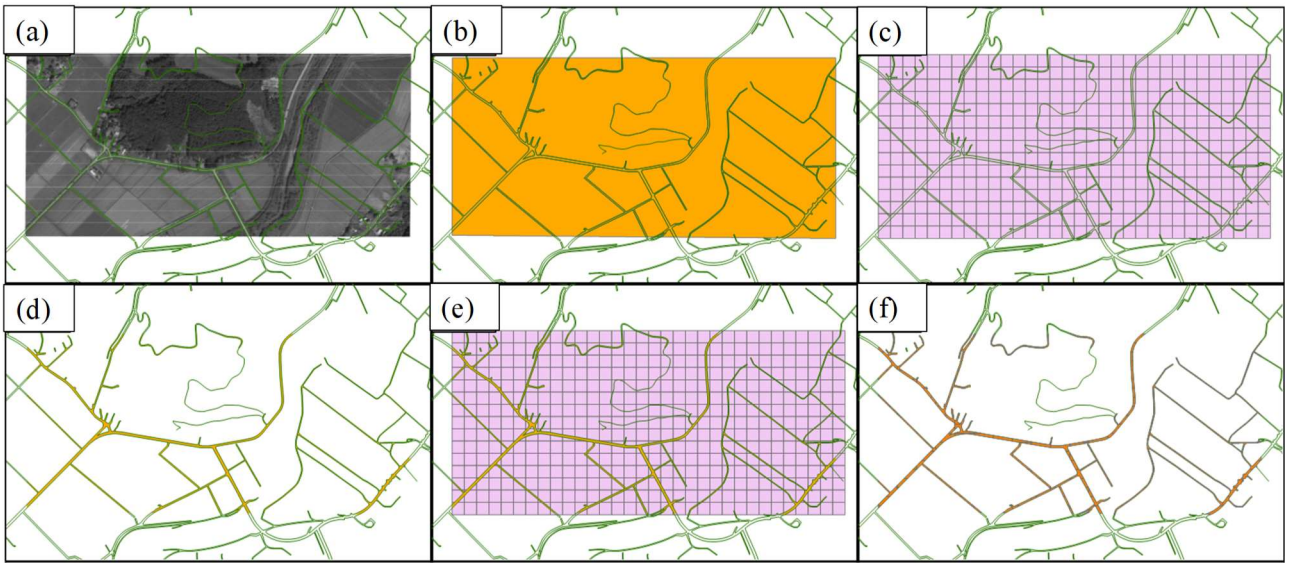

Fig. 1 Six-step process of construction of mesh data for road areas.

3. Damage classification and characteristic values for analysis

Focusing on 17 slope failures and 3 road failures in the selected aerial photographs, we classified the features of these seven geometrically corrected grey-scale images into three categories: (A) uniformly dark luminance distributed around the damaged parts of a targeted road, (B) dark luminance within damaged parts of a targeted road with bright luminance surrounding the damaged areas and (C) uniformly bright luminance around the damaged areas.

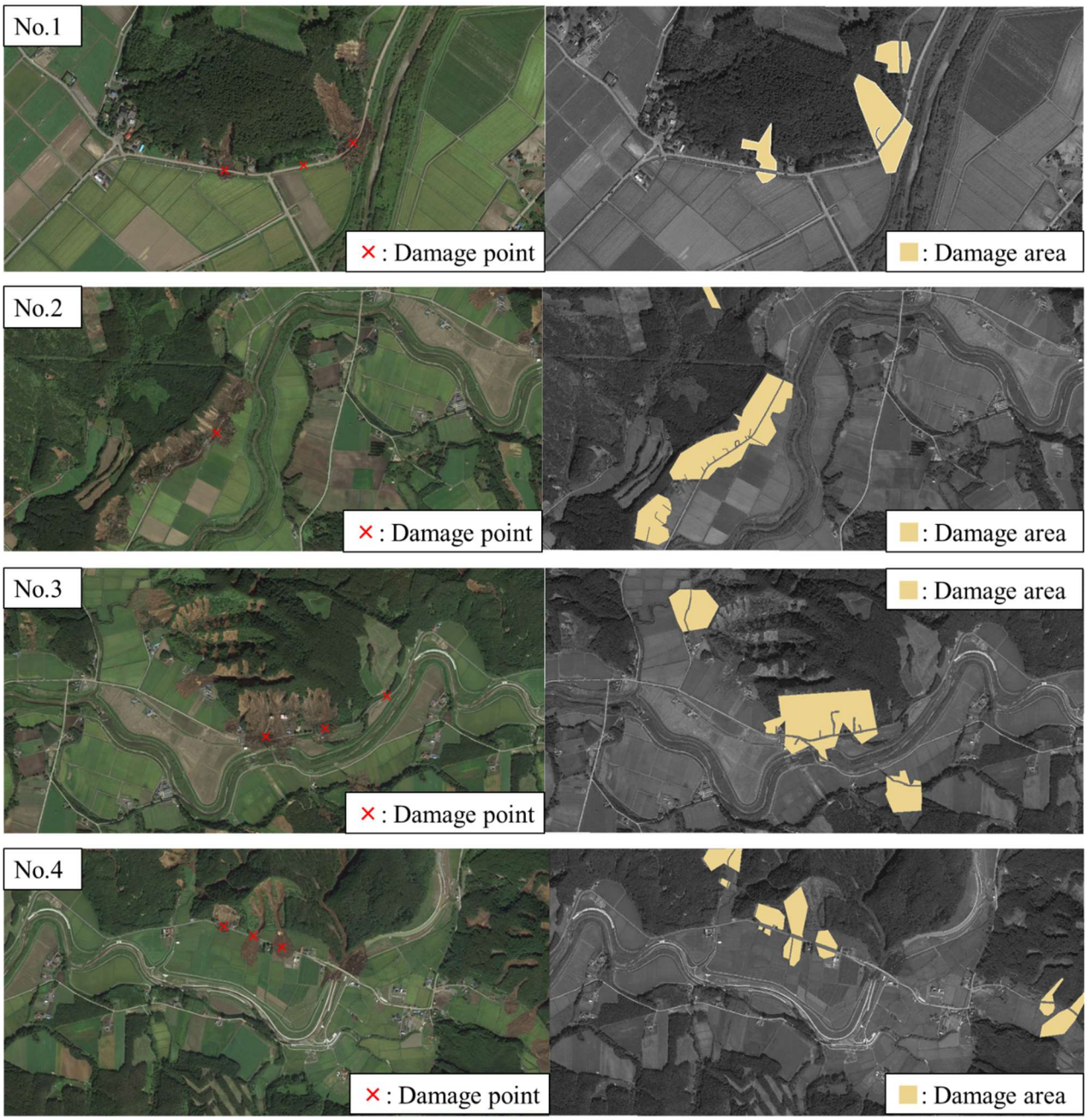

Fig. 2 Aerial photographs No. 1 through No. 4 with damage points and damage area polygons in geometrically corrected monochrome aerial photographs.

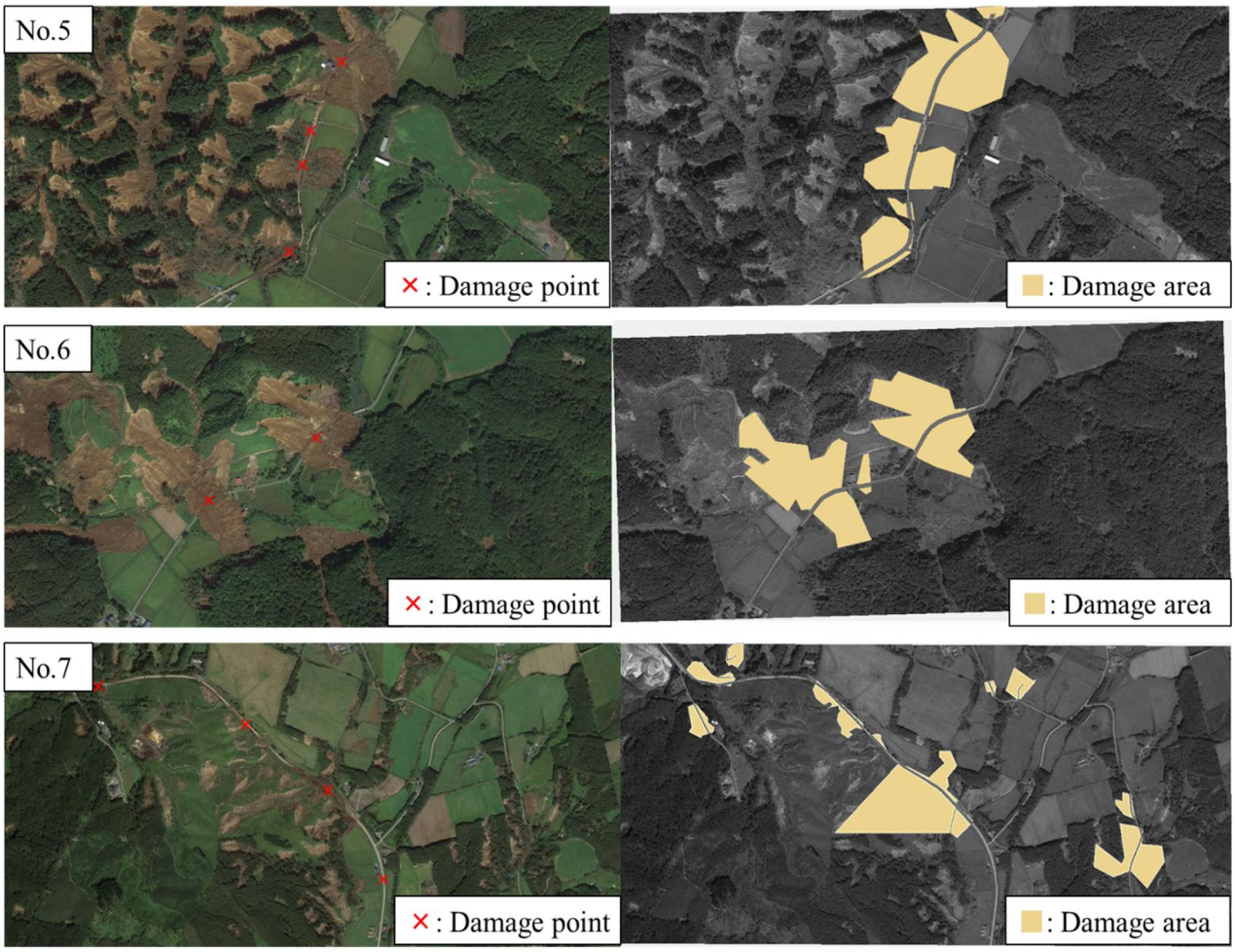

Fig. 3 Aerial photographs No. 5 through No. 7 with damage points and damage area polygons in geometrically corrected monochrome aerial photographs.

First, we defined the mean value about luminance l of 0~255 and the probability mass functions $P(l)$ as shown in equation (1a). The six indices used for the characteristic values quantifying the luminance of monochromatic images - contrast (*CNT*), variance (*VAR*), skewness (*SKW*), kurtosis (*KRT*), energy (*EGY*) and entropy (*EPY*) - can be represented in equations (1b) - (1g):

$$MEN = \sum_{l=0}^{255} l \cdot P(l) \tag{1a}$$

$$CNT = \sum_{l=0}^{255} l^2 \cdot P(l) \tag{1b}$$

$$VAR = \sum_{l=0}^{255} (l - MEN)^2 \cdot P(l) \tag{1c}$$

$$SKW = \frac{1}{VAR^{\frac{3}{2}}} \sum_{l=0}^{255} (l - MEN)^3 \cdot P(l) \tag{1d}$$

$$KRT = \frac{1}{VAR^2}\sum_{l=0}^{255}(l - MEN)^4 \cdot P(l) \tag{1e}$$

$$EGY = \sum_{l=0}^{255} P^2(l) \tag{1f}$$

$$EPY = -\sum_{l=0}^{255} P(l) \cdot \log_N P(l) \tag{1g}$$

Equations (1f) and (1g) show that *EGY* and *EPY* have opposite characteristics. Based on the previous research [6], by using texture analysis and 27 pixel * pixel windows targeting only road pixels, we generated histograms of the six characteristic values for each of the seven aerial photographs (Fig. 4). Only *SKW* can be <0, so pixels not computed are blue with representing the value 0.

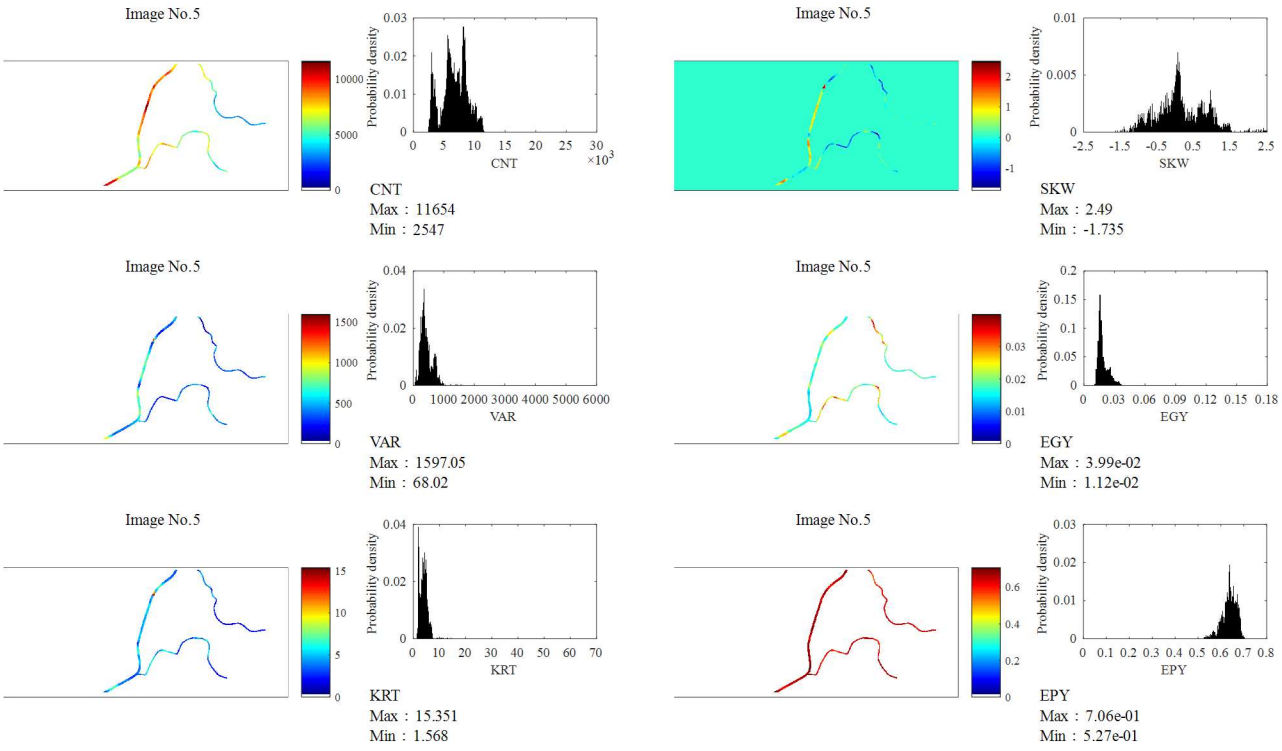

Fig. 4 Histograms of contrast (*CNT*), variance (*VAR*), kurtosis (*KRT*), skewness (*SKW*), energy (*EGY*) and entropy (*EPY*) for image No. 5.

4. Characteristic values at damage points and calculation of thresholds

At each damage point (Fig. 2), the Category A characteristic values of *CNT*, *VAR*, *SKW* and *EPY* (Table 1) are highly explainable with mean values 5956, 233.30, 0.319 and 0.604, respectively.

To determine the boundary between a damaged-road pixel and an undamaged one, we assumed a threshold value for each characteristic value. Then, for each image, we calculated differences between the assumed threshold value and the characteristic value for each damaged-road pixel and summed up all for each damaged-road pixel. Finally, we optimised the threshold values by minimising the sums of squares of the above differences.

Table 1 Characteristics values at damage points and damage classification (*CNT*, contrast; *EGY*, energy; *EPY*, entropy; *KRT*, kurtosis; *SKW*, skewness; *VAR*, variance)

Number of Images	Number of damage points	Failure mode	Damage length [m]	Coordinate(x,y)		Size of Images(x,y)		*CNT*	*VAR*	*KRT*	*SKW*	*EGY*	*EPY*	Categories of images
1	1-1	Slope failure	70	428	310	1051	498	6861	947.2	3.917	1.077	0.0131	0.689	B
	1-2	Road failure	-	544	311			10326	718.3	2.95	0.480	0.0145	0.673	C
	1-3	Slope failure	200	675	271			6011	734.49	3.7	0.891	0.0133	0.686	B
2	2-1	Slope failure	85	448	223	1052	494	5587	195.86	4.814	0.215	0.0237	0.599	A
3	3-1	Slope failure	100	508	329	1049	513	5022	304.98	6.76	1.465	0.0233	0.611	A
	3-2	Slope failure	81	634	312			5326	252.07	2.924	-0.015	0.0194	0.623	A
	3-3	Road failure	-	779	212			10002	462.17	3.103	0.235	0.015	0.664	C
4	4-1	Slope failure	30	430	153	1049	518	8240	434.95	7.598	0.848	0.016	0.655	B
	4-2	Slope failure	30	478	172			7126	207.92	5.712	0.246	0.0253	0.594	A
	4-3	Slope failure	60	532	190			6406	82.96	4.396	-0.066	0.0342	0.538	A
5	5-1	Slope failure	42	444	422	1036	469	6158	329.18	4.32	0.042	0.0194	0.633	A
	5-2	Slope failure	39	504	255			7970	322.79	4.582	0.371	0.0192	0.63	B
	5-3	Slope failure	20	519	201			9258	514.15	4.834	0.879	0.0193	0.651	C
	5-4	Slope failure	200	567	86			8686	328.42	5.464	-0.074	0.0206	0.628	A
6	6-1	Slope failure	100	337	274	1020	440	3519	212.83	2.286	0.846	0.0197	0.612	A
	6-2	Slope failure	210	535	146			11547	721.41	2.51	0.659	0.0129	0.685	B
7	7-1	Road failure	-	648	381	1050	491	9031	401.37	6.37	1.573	0.0274	0.598	B
	7-2	Slope failure	350	528	222			5772	185.51	3.124	0.210	0.0221	0.602	A
	7-3	Slope failure	140	386	105			7486	547.83	5.39	1.242	0.0196	0.642	B
	7-4	Slope failure	290	188	65			5673	387.26	6.727	1.387	0.0216	0.626	B

Table 2 Mean and standard deviation of characteristic values (*CNT*, contrast; *EPY*, entropy; *SKW*, skewness; *VAR*, variance)

Image No.	*CNT*	*VAR*	*SKW*	*EPY*
1	7300	670	0.661	0.671
2	6300	400	0.566	0.641
3	7100	440	0.661	0.637
4	7000	270	0.277	0.584
5	7700	450	0.186	0.626
6	9300	350	0.356	0.625
7	6600	380	0.615	0.636
Average	7357	423	0.475	0.633
Standard deviation	910	115	0.183	0.0239

5. Damage detection and its validity

A detected damaged-road pixel satisfies the following:

$$C_{avg} - \sigma \leq C_r \leq C_{avg} + \sigma \tag{2}$$

where C_r is the characteristic value of a road pixel, C_{avg} is the mean of the threshold values and σ is the standard deviation.

By comparing Figs. 5 and 2, it is apparent that Category A damage points (framed in blue) as well as Categories B and C damage points (framed in red) are all correctly detected. Hence, the C_{avg} value for *EPY* can accurately detect most of the damage points. However, areas framed in green contain pixels where roads are shadowed by forest and thus are not well detected as damage points. And damage detection for Image No. 6 is not enough to guarantee the accuracy, then we do not deal with the result in the following Figures.

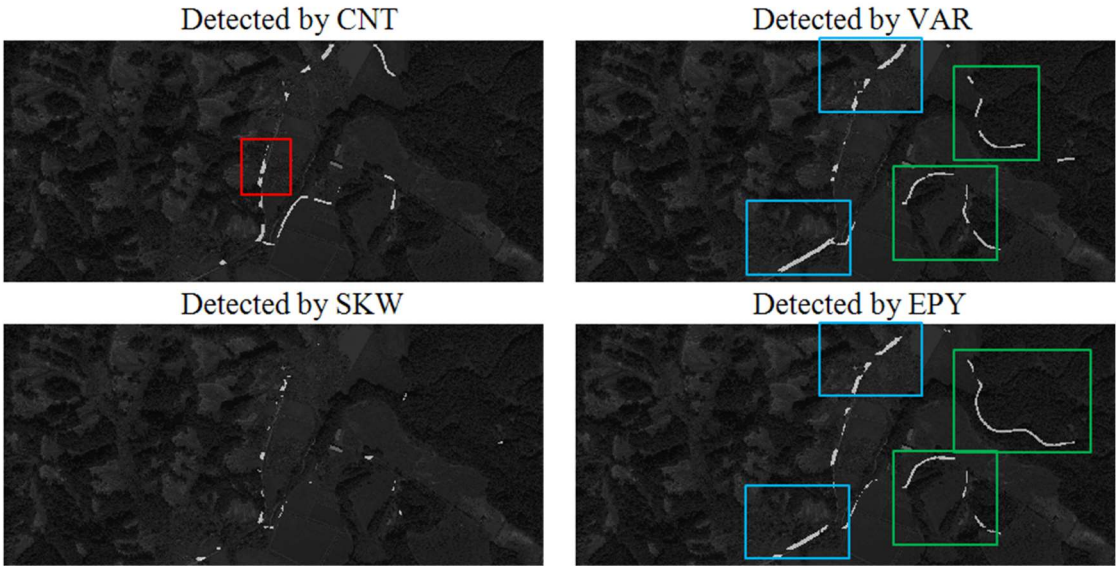

Fig. 5 Damage detection for image No. 5 by characteristic values of contrast (*CNT*), variance (*VAR*), skewness (*SKW*) and entropy (*EPY*).

To verify the validity of the damage detection, we classified the road-pixels data into four types (Table 3): actual damaged-road pixel detected as damaged (true positive, *TP*), actual damaged-road pixel detected as undamaged (false negative, *FN*), undamaged-road pixel detected as damaged (false positive, *FP*) and undamaged-road pixel detected as undamaged (true negative, *TN*). We used the evaluation indices *Recall*, *Precision*, *F-measure* and *Accuracy* to verify damage-detection validity (Table 4; Fig. 6). We selected *Recall* and *Accuracy* as the most explanatory indices for verifying validity.

Table 3 Category of road pixel (*FN*, false negative; *FP*, false positive; *TN*, true negative; *TP*, true positive)

		Damage detection	
		Damage	No damage
Actual damage	Damage	*TP*	*FN*
	No damage	*FP*	*TN*

Table 4 Indices for verifying validity of damage detection (*FN*, false negative; *FP*, false positive; *TN*, true negative; *TP*, true positive)

Evaluation index	Calculation formula
Recall	$\frac{TP}{TP+FN}$
Precision	$\frac{TP}{TP+FP}$
F-measure	$\frac{2}{\frac{1}{Recall}+\frac{1}{Precision}}$
Accuracy	$\frac{TP+TN}{TP+FN+FP+TN}$

According to the *Recall* index, the highest mean value is that of *EPY* (38%), which could be a value limiting the validity of such damage detection. In contrast, mean values for the *Accuracy* index are in the range 68% - 78%, which guarantees a high level of accuracy by this damage-detection procedure.

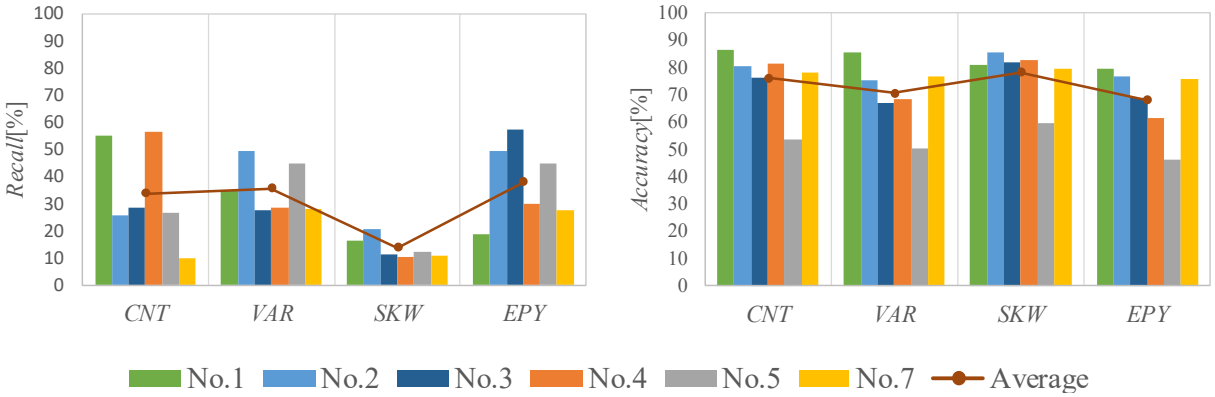

Fig. 6 *Recall* and *Accuracy* of characteristic values contrast (*CNT*), variance (*VAR*), skewness (*SKW*) and entropy (*EPY*).

6. Conclusions

Damaged-road images after the 2018 Hokkaido Iburi-Tobu earthquake were based on seven aerial photographs obtained from the Google Disaster Information Map and damage detection using explanatory indices: contrast, variance, skewness and entropy as characteristic values to quantify the luminance of the derived monochromatic images. We found that the validity of damage detection using entropy was the highest but the average value of the *Recall* reached a maximum of only <40%. For future studies, we would reconsider the method of determining threshold values and of setting their range limits.

7. Acknowledgment

The authors gratefully acknowledge Hokkaido Government and Japan Society of Civil Engineers for providing various data about road damages on the Hokkaido Iburi-Tobu earthquake. The support by JSPS KAKENHI Grant Number JP 17H01287 is gratefully acknowledged. The authors would like to thank MARUZEN-YUSHODO Co., Ltd. (https://kw.maruzen.co.jp/kousei-honyaku/) for the English language editing.

8. Reference

[1] Midorikawa S, Miura H (2010): Extraction of landslide areas due to the 2008 Iwate-Miyagi-Nairiku, Japan Earthquake from high-solution SAR Image, *Journal of Japan Association for Earthquake Engineering*, **10**(3), 25-32.

[2] Shoji G, Sakurai T (2011): Analysis on failure modes of road structures due to the slope failures in the 2008 Iwate-Miyagi earthquake and development of the related damage function, *Journal of Japan Association for Earthquake Engineering*, **11**(5), 94-106.

[3] Yoshinari K, Shoji G (2019): Damage detection of road structures due to the 2018 Hokkaido Iburi Tobu earthquake, *Proceeding of JCOSSAR 2019*, 292-297.

[4] Ministry of Land, Infrastructure, Transport and Tourism: *The basic map information of Geospatial Information Authority of Japan*. https://fgd.gsi.go.jp/download/menu.php.

[5] Google: *Google Disaster Information Map*. http://google.org/crisismap/google.com/2018-hokkaidoearthquake.

[6] Miura H, Midorikawa S, Chen S H (2012): Texture analysis of high-resolution satellite images for damage detection in the 2010 Haiti earthquake, *Journal of Japan Association for Earthquake Engineering*, **12**(6),2-20.

